Microhydrodynamics of Sharp Corners and Edges: Traction Singularities

I. Mustakis and S. Kim
Dept. of Chemical Engineering, University of Wisconsin, Madison, WI 53706

Sharp corners and edges are ubiquitous in modern technology and found on the tip of an atomic force microscope (AFM) and the vertices and edges of crystalline materials. The microhydrodynamics of particles with sharp corners and edges are special in that geometric discontinuities give rise to traction singularities for viscous flow around the particles. Such traction fields are analyzed with both analytical and numerical solution of a second kind integral equation. The traction field in the vicinity of a vertex has a singular structure that is more intricate than simple superposition of the well-known edge singularities. The new insights into the structure of the vertex singularities are used to formulate and test spectral element strategies for numerical solution of viscous flow past sharp corners and edges. The best schemes constructed to date show remarkable agreement with the analytical results.

Introduction

Particles with sharp corners and edges are ubiquitous in natural and manufacturing processes (clay minerals and compound semiconductors to name two examples). Because of the underlying materials chemistry, the corners and edges may be viewed as "sharp" to atomistic scales. The present work provides a framework for the theoretical investigation of the dynamics of such particles in a viscous fluid, with special emphasis on the analysis of the traction field developed on their surfaces. Our work is thus relevant to the analysis of hydrodynamic interactions between surfaces with sharp corners and edges such as the viscous component of the force balance on an AFM tip. Furthermore, knowledge of traction singularities for Stokes flow past the edges can be exploited by the CFD community for validation of more general Navier-Stokes solvers, as in Karniadakis (1989) and the design of more robust numerical techniques for such geometries (Georgiou et al., 1990; Pathria and Karniadakis, 1995).

A half-century ago two chemical engineers, Pettyjohn and Christiansen, conducted the definitive set of experiments on the sedimentation velocities of small particles with sharp corners and edges and published their findings (Pettyjohn and Christiansen, 1948). Even to this day, the conventional procedures for accounting for shape effects (via sphericity corrections) can be traced back to this oft-cited work. In the present work we are able not only to predict the sedimentation velocities of such particles or equivalently the hydrodynamic drag for a given uniform stream, but also the actual distribution of viscous stresses on the particle surface including the singular nature of the vertex and edge regions.

One-third of a century has elapsed since the publication of Howard Brenner's (1964) seminal work on the Stokes drag on a particle of arbitrary shape in arbitrary fields of flow. Brenner showed that the drag on a particle in an arbitrary flow field was related to the tractions on the same particle in rigid body motion through an otherwise quiescent fluid. Knowledge of the latter allowed computation of the former, as a consequence of the Lorentz reciprocal theorem (Happel and Brenner, 1983). More recently, it has been shown that Brenner's idea can be used in *reverse*, that is, knowledge of the drag on a particle in an arbitrary flow field in combination with the Riesz representation theorem provides the requisite information to construct the traction field for a particle in rigid body motion (Karrila, 1988). For this reason, Pakdel and Kim (1996) refer to the new integral equation for the tractions as the *Riesz-Rennerb equation.*

The presence of geometric discontinuities such as corners and edges is associated with singular behavior of the stress and traction fields in both hydrodynamic (Moffatt, 1964) and elasticity problems (Williams, 1952). Two decades ago, the first solutions (based on a finite difference formulation) appeared for the stress field in the closely-related problem of

Correspondence concerning this article should be addressed to S. Kim at the present address: Scientific Information Resources, Parke-Davis Pharmaceutical Research, 2800 Plymouth Road, Ann Arbor, MI 48105.

elastic semi-infinite cracks in the half-space (Benthem, 1977). Benthem's ideas can be reformulated in the context of the Riesz-Rennerb integral equation; upon combination with recent advances in asymptotic methods for hypersingular integrals (Rosen and Cormack, 1995), we obtain a new understanding and complete picture of the nature of traction singularities at the vertices of a polyhedral particle in a viscous flow field.

The completed double layer integral representation for the velocity fields of the Stokes flow is used as the starting point for an analysis. The Riesz-Rennerb equations for the tractions are also introduced with a brief sketch of the derivation relegated to Appendix. The continuation approach is introduced for the analysis of singular integrals and its application to the Riesz-Rennerb equations. This analysis extracts the singular behavior of the tractions near vertices and edges directly from the integral equation. This shows explicitly that the integral equation can be applied to problems with sharp features. Previously unknown traction exponents for the vertex region are deduced. The various boundary element discretization techniques are introduced and described, namely, lower order, spectral and B-Spline elements, to set the stage for future articles. Results are presented from BIEM simulations of the Riesz-Rennerb equation. The singular traction field for a cube is examined and the singular exponents for both edges and corners are extracted from the numerical results and compared with analytical results. This introductory exposition is concluded with a brief overview of the implications for future works on microhydrodynamics of sharp corners and edges.

Integral Equation for Tractions

Consider a set of N small rigid particles of arbitrary shape moving through a viscous incompressible fluid in reaction to an external force $\boldsymbol{F}^{(\nu)}$ and external torque $\boldsymbol{T}^{(\nu)}$ acting on the particles. Furthermore, the shape of the particle ν, ($\nu = 1, 2, \ldots, N$) is described by the set of points ξ that make up its surface $S^{(\nu)}$. The system under consideration is such that if the particles were not moving, the fluid would be quiescent. However, the motion of the particles creates a disturbance velocity in the fluid domain. From standard texts in chemical engineering (Bird et al., 1960; Happel and Brenner, 1983), we know that the disturbance velocity $\boldsymbol{v}$ and pressure p fields are governed by the Stokes equations

$$-\nabla p + \mu\nabla^2\boldsymbol{v} = \boldsymbol{0}, \quad \nabla\cdot\boldsymbol{v} = 0 \tag{1}$$

because the Reynolds number $\rho|\boldsymbol{v}|\,\ell/\mu$ in the system under consideration is vanishingly small. Here, μ and ρ denote the viscosity and density of the fluid. The constant gravitational force in the fluid has been incorporated into the pressure field in Eq. 1.

In general, the objective is to solve Eq. 1 to determine the motion of the particles and the value of the velocity field throughout the fluid domain. Over the past decade, considerable progress has been made in this fundamental problem of microhydrodynamics. The derivation of the computational methodology and examples for particles of various shapes are readily available in Kim and Karrila (1991) and Pozrikidis (1991) and will not be repeated here.

Table 1. Traction Exponents for the 90° Vertex

Flow	Exponent
Symmetric	0.31877
Antisymmetric	0.62463

The final results can be summarized as follows. The velocity field in the fluid domain is given by an integral representation in terms of an unknown dipole density function $\boldsymbol{\varphi}(\xi)$ distributed over the particle surface $S^{(\nu)}(\xi)$

$$\boldsymbol{v}(\boldsymbol{x}) = -\sum_{\nu=1}^{N}\left[\boldsymbol{F}^{(\nu)} - \frac{1}{2}(\boldsymbol{T}^{(\nu)}\times\nabla)\right]\cdot\frac{\mathcal{G}(\boldsymbol{x},\boldsymbol{x}_c^{(\nu)})}{8\pi\mu} + \oint_S \boldsymbol{K}(\boldsymbol{x},\xi)\cdot\boldsymbol{\varphi}(\xi)\,dS(\xi), \tag{2}$$

where the surface integral is over all particle surfaces and the kernel $\boldsymbol{K}$ is given by

$$\boldsymbol{K}(\boldsymbol{x},\xi) = -2\boldsymbol{n}(\xi)\cdot\Sigma(\boldsymbol{x},\xi) = \frac{3}{2\pi}\frac{(\boldsymbol{x}-\xi)(\boldsymbol{x}-\xi)(\boldsymbol{x}-\xi)\cdot\boldsymbol{n}(\xi)}{|(\boldsymbol{x}-\xi)|^5}.$$

Here $\boldsymbol{n}$ is the normal vector pointing outward of the particle, $\boldsymbol{x}_c^{(\nu)}$ is the center of particle ν and $\Sigma(\boldsymbol{x},\xi)$ is the stress field of the Oseen-Burgers tensor

$$\mathcal{G}(\boldsymbol{x},\xi) = \frac{\boldsymbol{\delta}}{|(\boldsymbol{x}-\xi)|} + \frac{(\boldsymbol{x}-\xi)(\boldsymbol{x}-\xi)}{|(\boldsymbol{x}-\xi)|^3}.$$

The dipole density $\boldsymbol{\varphi}$ is determined by solving a Fredholm integral equation of the second kind

$$\boldsymbol{\varphi} + \oint_S\left(\boldsymbol{K} + \sum_{\nu,i}\boldsymbol{\varphi}^{(\nu,i)}\boldsymbol{\varphi}^{(\nu,i)}\right)\cdot\boldsymbol{\varphi}\,dS = \boldsymbol{b}, \tag{3}$$

with

$$\boldsymbol{b} = -\boldsymbol{v}^{\infty} - \sum_{\nu=1}^{N}\left[\boldsymbol{F}^{(\nu)} - \frac{1}{2}(\boldsymbol{T}^{(\nu)}\times\nabla)\right]\cdot\frac{\mathcal{G}(\boldsymbol{x},\boldsymbol{x}_c^{(\nu)})}{8\pi\mu}, \tag{4}$$

where $\boldsymbol{\varphi}^{(\nu,i)}$ are the six orthonormalized rigid body velocities of the particle ν as described in Kim and Karrila (1991). Iterative numerical methods that exploit the properties of second kind integral equations are applied on Eq. 3.

The density function $\boldsymbol{\varphi}$ also appears in relatively simple, closed-form expressions that yield the three translational and rotational velocity components that describe the movement of the particle

$$\left.\begin{aligned} U_i^{(\nu)} &= -\frac{1}{\sqrt{S^{(\nu)}}}\langle\boldsymbol{\varphi}^{(\nu,i)},\boldsymbol{\varphi}\rangle \\ \omega_i^{(\nu)} &= -\frac{1}{\sqrt{I_i^{(\nu)}}}\langle\boldsymbol{\varphi}^{(\nu,i+3)},\boldsymbol{\varphi}\rangle \end{aligned}\right\}, \quad i = 1,\ldots,3 \quad \text{and} \quad \nu = 1,\ldots,N \tag{5}$$

where

$$I_i^{(\nu)} = \int_{S(\nu)} \left[\boldsymbol{r}^{(\nu)} \cdot \boldsymbol{r}^{(\nu)} - \left(r_i^{(\nu)} \right)^2 \right] dS$$

are the moments of inertia of particle surface about the ith coordinate and $\boldsymbol{r}^{(\nu)} = \boldsymbol{x} - \boldsymbol{x}_c^{(\nu)}$ is the position vector from the particle's surface to center.

The objective of this article is to find appropriate extensions of the methodology when sharp corners and edges are present and to elucidate the nature of the surface traction $\boldsymbol{t} = \boldsymbol{\sigma} \cdot \boldsymbol{n}$ on such particles. From our knowledge of the stress field $\boldsymbol{\sigma}$ on corners and edges of a particle surface, we gain new insights into the crafting of a special numerical method for computing hydrodynamic interactions between sharp surfaces. Therefore in this introductory article, we digress from the analysis of the above integral equations and focus our attention on the analysis of the *Riesz-Rennerb* internal equation.

Karrila (1988) pioneered the idea of combining the Riesz representation theorem with Brenner's work on particles of arbitrary shape (Brenner, 1964). In essence, instead of assuming knowledge of $\boldsymbol{t}$ to obtain expressions for the hydrodynamic drag in arbitrary flows, Brenner's flow of information is *reversed*: a method for computing the drag in arbitrary flow fields yields the expression for $\boldsymbol{t}$. For this reason, Pakdel and Kim (1996) have named Eq. 6 the *Riesz-Rennerb equation*. The Riesz-Rennerb equation,

$$\boldsymbol{t} + \oint_S \left(\boldsymbol{K}^* + \sum_{\nu,i} \boldsymbol{\varphi}^{(\nu,i)} \boldsymbol{\varphi}^{(\nu,i)} \right) \cdot \boldsymbol{t} \, dS = \sum_{\nu=1}^{N} \left(\frac{\boldsymbol{F}^{(\nu)}}{S^{(\nu)}} + \frac{\boldsymbol{T}^{(\nu)} \times \boldsymbol{r}^{(\nu)}}{I^{(\nu)}} \right). \tag{6}$$

contains explicitly the link between the surface traction $\boldsymbol{t}$ and the external forces and torques on the particles. Note that if $\boldsymbol{t}$ is the only quantity of interest, the problem of determining $\boldsymbol{v}$ and particle motion $\boldsymbol{U}^{(\nu)} + \boldsymbol{\omega}^{(\nu)} \times \boldsymbol{r}^{(\nu)}$ can be bypassed altogether! *This is a remarkable result that has not yet been digested outside the narrow strata of specialists in microhydrodynamics research.*

In Eq. 6, the kernel $\boldsymbol{K}^*$ is the adjoint kernel of $\boldsymbol{K}$ and is defined in the usual fashion

$$K_{ij}^*(\boldsymbol{x}, \boldsymbol{\xi}) = K_{ji}(\boldsymbol{\xi}, \boldsymbol{x}).$$

The formal derivation of the Riesz-Rennerb equation is nontrivial, but is available in great detail in part IV of Kim and Karrila (1991). A concise version from the work of Kim and Power (1993) is reproduced in the Appendix.

Continuation Analysis near Edges and Vertices

In this section we apply the continuation approach for singular integration developed by Rosen and Cormack (1995) and Cormack and Rosen (1996) to the integrals that appear in the Riesz-Rennerb equation. We shall see that such an analysis applied to the edge and vertex regions yields the functional form of the singularities of the traction field.

We also recast the physical problem from that of a particle moving in a quiescent fluid to that of a fixed particle in a uniform stream. The two problems are mathematically equivalent, but the latter viewpoint facilitates direct comparison with well-known classical stream function analyses for flows impinging upon a wedge.

Edges

Consider an edge formed by two adjacent planar surfaces, as shown in Figure 1. This problem furnishes a useful test case as the singular nature of the tractions can be deduced from the classical two-dimensional stream function solution for flow past a wedge. (That analysis shows tractions on the point P' a distance ϵ away from the edge become unbounded as ϵ^{-p}, in the limit as the point P' approaches the edge.) Once we fix the boundary conditions as no-slip, the exponent p depends only on the dihedral angle. We now show that an asymptotic analysis of the dominant terms in the Riesz-Rennerb equation yields the same information. Although our approach works for all dihedral angles, we showcase only the analysis for the 90° angle, as the requisite integrals have nice closed-form solutions. The particle in question, then, is a cube.

In the Riesz-Rennerb equation, only the integral with the integrand $K_{ij}^*(\boldsymbol{x}, \boldsymbol{\xi}) t_j(\boldsymbol{\xi})$ exhibits singular behavior. Furthermore, that singular behavior is limited to one region: the portion of the adjacent face nearest to P', so we focus our attention on the surface integral over the "top" face in Figure 1, that is, the $\xi_1 \xi_2$ plane. In the region near the edge, we apply the leading order behavior for the tractions

$$t_j(\boldsymbol{\xi}) \sim c_j \xi_1^{-p}$$

and define

$$K_{ij}^*(\boldsymbol{x}, \boldsymbol{\xi}) c_j \xi_1^{-p} = \frac{-3}{2\pi} f_{ij}$$

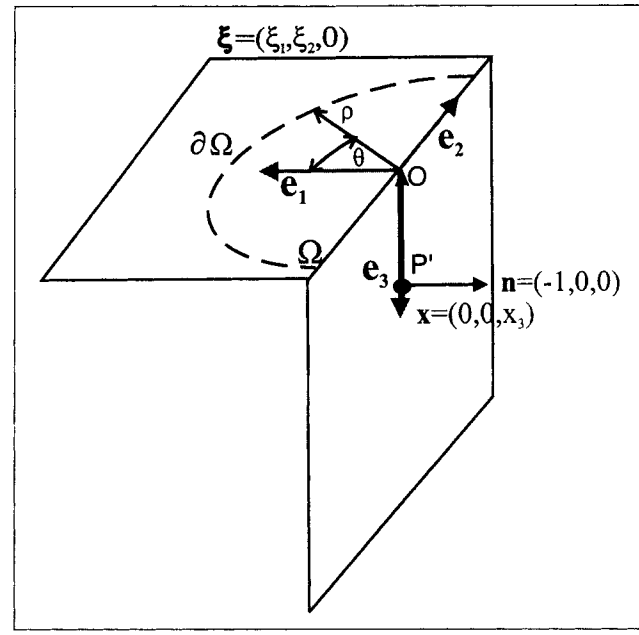

Figure 1. Edge: definition of the local coordinate systems, for the traction problem.

so that upon substitution of

$$\boldsymbol{\xi} = (\xi_1, \xi_2, 0), \quad \boldsymbol{x} = (0,0,x_3), \quad \boldsymbol{n} = (-1,0,0) \tag{7}$$

we obtain

$$f_{11} = \frac{\xi_1^{3-p}}{\left(\xi_1^2 + \xi_2^2 + x_3^2\right)^{5/2}}, \quad f_{12} = \frac{\xi_1^{2-p}\xi_2}{\left(\xi_1^2 + \xi_2^2 + x_3^2\right)^{5/2}},$$
$$f_{13} = -\frac{\xi_1^{2-p}x_3}{\left(\xi_1^2 + \xi_2^2 + x_3^2\right)^{5/2}}, \quad f_{22} = \frac{\xi_1^{1-p}\xi_2^2}{\left(\xi_1^2 + \xi_2^2 + x_3^2\right)^{5/2}},$$
$$f_{23} = -\frac{\xi_1^{1-p}\xi_2 x_3}{\left(\xi_1^2 + \xi_2^2 + x_3^2\right)^{5/2}}, \quad f_{33} = \frac{\xi_1^{1-p}x_3^2}{\left(\xi_1^2 + \xi_2^2 + x_3^2\right)^{5/2}} \tag{8}$$

These integrands for the top face are singular at the edge and thus require the analysis of Rosen and Cormack. Note that all integrals are of the form

$$I(z) = \int\int f(\xi_1, \xi_2, z)\, d\xi_1 d\xi_2$$

where f is a homogeneous function of degree $\beta = -2-p$, with respect to the variables ξ_1, ξ_2, and $z = x_3$. The integrand f is a C^∞ function for $(\xi_1, \xi_2, 0) \neq (0,0,z)$. However, it has a singular point at $(\xi_1, \xi_2, 0) = (0,0,z)$ as well as across the line $\xi_1 = 0$. In order to calculate the integral as $z \to 0$ we exploit the homogeneity of the integrand and Euler's identity.

$$\xi_1 \frac{\partial f}{\partial \xi_1} + \xi_2 \frac{\partial f}{\partial \xi_2} = \beta f - z \frac{\partial f}{\partial z}.$$

We integrate both sides, apply Green's theorem to the left-hand side to convert it to a line integral and rearrange terms to obtain

$$z \frac{\partial}{\partial z} I(z) - sI(z) = -\int_{\partial\Omega} f\boldsymbol{\xi} \cdot d\boldsymbol{l}, \tag{9}$$

where $s = \beta + 2 = -p$ is the degree of singularity when $(0,0,z) \in \partial\Omega$, $d\boldsymbol{l}$ is the directional boundary element. The case of $s > 0$ corresponds in general to convergent regular integrals; integrals with $s = 0$ are referred to as Cauchy-type integrals and those with $s < 0$ are known as hypersingular integrals. Equation 9 is an initial value problem which has the solution

$$I(z) = -z^s \int_{z_0}^{z} \left(\frac{1}{\eta^{s+1}} \int_{\partial\Omega} f(\boldsymbol{\xi}, \eta)\boldsymbol{\xi} \cdot d\boldsymbol{l} \right) d\eta + \frac{z^s}{z_0^s} I(z_0). \tag{10}$$

We can now calculate the value at the point $z = 0$ (edge) in terms of its value at a point z_o away from the vertex plus a double integral across a semicircular region radiating from the singular point as shown in Figure 1.

By letting $z_0 = \pm\infty$ for all s we have

$$I(z) = z^s \int_{\partial\Omega} \{F_\infty(\boldsymbol{\xi}) - F(\boldsymbol{\xi}, z)\}\boldsymbol{\xi} \cdot d\boldsymbol{l} \tag{11}$$

where

$$F(\boldsymbol{\xi}, z) = \int \frac{1}{z^{s+1}} f(\boldsymbol{\xi}, z)\, dz \tag{12}$$

is the primitive boundary function (PBF) (Rosen and Cormack, 1995) and F_∞ is the limit of F for $z_0 \to \infty$. The necessary and sufficient conditions for the integral to be bounded depend on the value of s and are

$$\mathrm{Res}I = \int_{\partial\Omega} f(\boldsymbol{\xi}, 0)\boldsymbol{\xi} \cdot d\boldsymbol{l} = 0, \quad \text{for } s = 0 \tag{13}$$

where Res$I$ denotes the residue of the integral and

$$GfI = \int_0^\infty \left\{ \frac{1}{\eta^{s+1}} \int_{\partial\Omega} f(\boldsymbol{\xi}, \eta)\boldsymbol{\xi} \cdot d\boldsymbol{l} \right\} d\eta$$
$$= \int_{\partial\Omega} \{F_\infty(\boldsymbol{\xi}) - F(\boldsymbol{\xi}, 0)\}\boldsymbol{\xi} \cdot d\boldsymbol{l} = 0, \quad \text{for } s < 0. \tag{14}$$

The notation GfI denotes the gauge functional applied to the integral I. This condition is defined as the gauge condition by Rosen and Cormack (1995). If the gauge conditions are not satisfied the integrals will diverge as $z \to 0$

$$\lim_{z \to 0} I(z) = \begin{cases} (GfI)\dfrac{1}{z^{-s}}, & s < 0 \\ (\mathrm{Res}I)\log|z|, & s = 0. \end{cases} \tag{15}$$

Both the residual and the gauge functionals are independent of the integration path. We can now apply the continuation approach separately in each of the planes that create the vertex. One major simplification when working with flat domains is that the only surviving contribution to the line integral of Eq. 11 comes from the contour sweeping across the adjacent surface, such as the semicircular arc in Figure 1. The line integral along the edge is either identically zero or is canceled by integrals from the other surfaces.

We digress briefly to show that the assumption of nonsingular tractions ($p = 0$) leads to a contradiction. If $p = 0$, then $s = 0$, leading to Cauchy integrals; the integrals defined for f_{11}, f_{12}, and f_{22} will exhibit logarithmic singularity as $z \to 0$. However, due to the application of Eq. 6 and the assumption of smooth $\boldsymbol{t}$ this is impossible.

Classical 2-D analysis

Before evaluation of the integrals and the resulting conditions on the c_j, we now remind ourselves of the expected results by recalling the classical stream function result for flow past a wedge. The first local analysis of such flows was done by Dean and Montagnon (1949); the flow field around the wedge was expressed in polar coordinates centered on the corner

$$\psi(r, \theta) = \sum_\gamma r^\gamma g_\gamma(\theta). \tag{16}$$

Here γ is a complex number to be determined by the solution of an eigenvalue problem produced by Eq. 16 from the

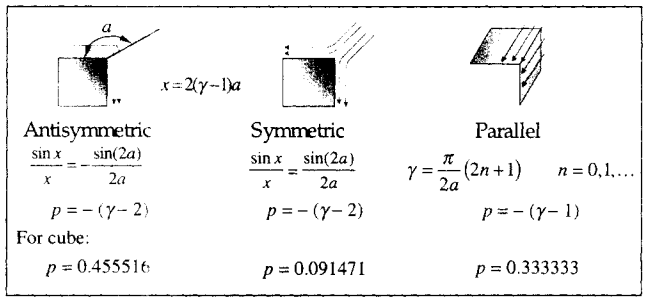

Figure 2. Classical 2-D analysis for flows around edges.

application of the boundary conditions. This will give a sequence of eigenvalues. The eigenvalues that are less than 2 are the ones that will produce singular behavior in the stress field. Dean and Montagnon (1949) and Moffatt (1964) showed that with no-slip boundary conditions the eigenvalue problem leads to

$$\sin 2a(\gamma-1) = \pm(\gamma-1)\sin 2a. \tag{17}$$

The definition of the angle a is given in Figure 2. The sign change corresponds to the *symmetric* (+) and *antisymmetric* (−) flows. The singularity is much stronger for the antisymmetric case, that is, $\gamma_{antisym} < \gamma_{sym}$. There is one additional flow of interest, namely unidirectional flow *parallel* to the edge. In this case a much simpler eigenvalue problem results. The velocity field can be written in the form

$$u_z(r,\theta) = \sum_{\gamma} r^{\gamma} f_{\gamma}(\theta).$$

The application of the boundary conditions produces a single sequence of eigenvalues. The eigenvalues with values less than 1 will produce singular stress fields. A summary of the classical two-dimensional (2-D) results are given in Figure 2. As we show below, we are able to reproduce the three singular traction exponents ($\gamma_{sym}-2$ for symmetric, $\gamma_{antisym}-2$ for antisymmetric, and $\gamma_{par}-1$ for parallel flows) from the continuation analysis of the boundary integral equation.

Results from the continuation method

If we presume that the exponent $p > 0$, the integrals of the Riesz-Rennerb equation become hypersingular. In order for the Riesz-Rennerb equation to be valid on the edge the following conditions must be satisfied by the coefficients of the traction

$$c_i' + \frac{3}{2\pi} GfI_{ij} c_j = 0,$$
$$c_i + \frac{3}{2\pi} GfI_{ij}' c_j' = 0. \tag{18}$$

The primed terms refer to the "side surface" entities. Here, GfI_{ij} are the individual gauge functionals of the kernel and the Einstein convention for index summation has been applied. Working with polar coordinates with the origin on the edge, we obtain analytic results for each gauge functional (this is why we considered a 90° dihedral angle)

$$GfI_{11} = \frac{2}{3}\Gamma\left(\frac{4-p}{2}\right)\Gamma\left(\frac{p}{2}\right),$$
$$GfI_{12} = GfI_{23} = 0,$$
$$GfI_{22} = \frac{1}{3}\Gamma\left(\frac{2-p}{2}\right)\Gamma\left(\frac{p}{2}\right),$$
$$GfI_{13} = \frac{2}{3}\Gamma\left(\frac{3-p}{2}\right)\Gamma\left(\frac{p+1}{2}\right),$$
$$GfI_{33} = \frac{2}{3}\Gamma\left(\frac{2-p}{2}\right)\Gamma\left(\frac{p+2}{2}\right). \tag{19}$$

Here $\Gamma(x)$ is the usual gamma function (Abramowitz and Stegun, 1970) and the gauge functional refers to the "top surface." Analogous entities exist for the "side surface." We denote these with a prime, and, by symmetry, we deduce

$$GfI_{11}' = GfI_{33},$$
$$GfI_{22}' = GfI_{22},$$
$$GfI_{33}' = GfI_{11},$$
$$GfI_{13}' = GfI_{13},$$
$$GfI_{12}' = GfI_{23},$$
$$GfI_{23}' = GfI_{12}. \tag{20}$$

We can see from Eq. 19 that the 12 and 23 gauge conditions are always satisfied. Thus, the 6×6 system (Eq. 18) can be decomposed into a 2×2 system and a 4×4 system. The former provides a condition for the exponent for the parallel mode of the flow, while the latter provides conditions for the exponent for the symmetric and antisymmetric modes.

- The 2×2 system immediately yields

$$GfI_{22} = \pm\frac{2\pi}{3} \Rightarrow p = 0.33333 \tag{21}$$

- The 4×4 system for the tractions normal to the edge

$$\begin{pmatrix} GfI_{11} & GfI_{13} & -2\pi/3 & 0 \\ GfI_{13} & GfI_{33} & 0 & -2\pi/3 \\ -2\pi/3 & 0 & GfI_{33} & GfI_{13} \\ 0 & -2\pi/3 & GfI_{13} & GfI_{11} \end{pmatrix} \begin{pmatrix} c_1 \\ c_3 \\ c_1' \\ c_3' \end{pmatrix} = 0 \tag{22}$$

has nontrivial solutions only for $p = -(\gamma-2) = 0.455516$ and $p = -(\gamma-2) = 0.091471$. These are precisely the same exponents obtained from the 2-D stream function solution.

The important conclusion is that the singular behavior of the tractions near the edge is of the form

$$t_i = c_{i1}\xi_1^{-p_1} + c_{i2}\xi_1^{-p_2} + c_{i3}\xi_1^{-p_3}. \tag{23}$$

The same analysis can be applied to other dihedral angles, but the gauge integrals require numerical integration. Figure

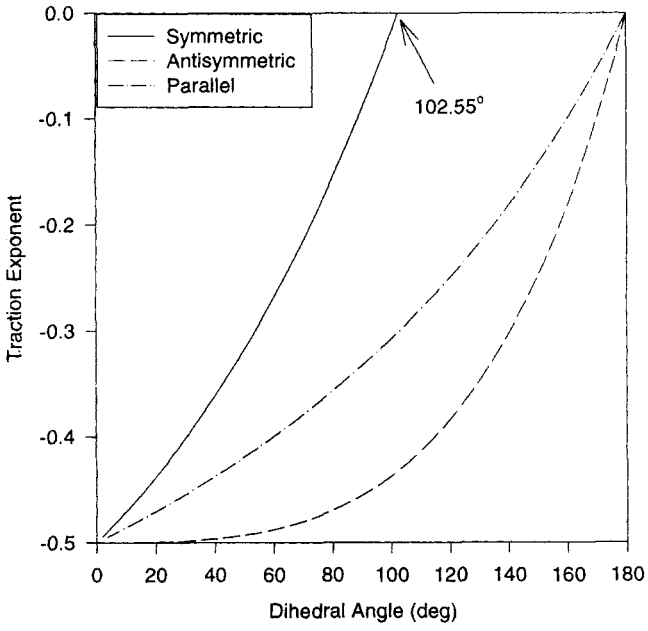

Figure 3. Traction exponents for flows around a 2-D edge calculated from the integral equation.

3 shows traction exponents as a function of dihedral angle as produced from the continuation analysis of the Riesz-Rennerb equation. Also from Figure 3 we can see that the antisymmetric flow always produces the higher singularities, followed by the parallel and symmetric flows, as expected from common intuition. Here, we should also mention that all three exponents approach -0.5 as the angle goes to 0°, reproducing the well known exponent for the 2-D crack problem in elasticity (Williams, 1952). The symmetric mode is singular only for dihedral angles less than 102.55°. For angles greater than 180° (plane), the singular behavior of both the parallel and antisymmetric modes disappears. Although not germane to the subject of this article, for angles greater than 200.89° and 213.7°, the symmetric and the antisymmetric modes produce, respectively, the so-called Moffatt eddies (Moffatt, 1964).

Vertices

It is intuitively obvious that the surface tractions at a 3-D vertex are at least as singular as those encountered at the edges, since a point near the vertex of a polyhedral surface is also near an edge. Furthermore, if we draw a small circular arc on a face near a vertex, we would also expect stronger singularities at the points of the arc near the edges, and a weaker singularity in the mid-regions of the arc well away from the edges ($\alpha = \pi/4$ and $\beta = \pi/4$ in Figure 4). Before solving the problem, we may venture a guess that the edges interact in some fashion to cause more singular behavior at the vertex regions. We will see the continuation method provides the definitive answer, of the form

$$t_i = r^{-q} \cos^{-p}\phi \sin^{-p}\phi H_i(\phi),$$

to support these intuitive ideas. The p exponents capture the edge singularities, while the q exponent is a feature of the vertex. Again, we stress that our method could be applied at any polyhedral vertex but is most easily illustrated for the cube.

Our work draws heavily from the mathematical analyses in the elasticity literature for 3-D cracks or notches, which involves the application of a variational principle in a sphere surrounding the vertex and discretization of the equations on the surface by finite differences (Benthem, 1980) or finite elements (Bažant and Estenssoro, 1979; Ghahremani, 1991; Nakamura and Parks, 1989). In the present work, we have a boundary integral equation so we discretize only the bounding arcs of the vertex boundary element, that is, we obtain the usual advantage of a boundary integral solution approach: all analyses are reduced in dimensionality by one.

The form of the singular tractions can be deduced by the general analysis of elliptic equations in conical or angular spaces as studied by Kondratev (1968). These equations admit separable solutions of the form $r^{\gamma} f(\theta, \phi)$ for the displacement field (elasticity) or velocity field (Stokes flow). Here r is the distance from the vertex. The exponent of the associated stress field is then $\gamma - 1$ from an application of the relevant constitutive equation. For Stokes flow, the no-slip boundary condition eliminates many terms in the constitutive equation, leading to the following form for the surface tractions

$$t(r, \phi) = r^{\gamma - 1} h(\phi) = r^{-q} h(\phi). \tag{24}$$

Here ϕ is the azimuthal angle spanning the surface of one of the planes of interest such as the xy plane that forms the

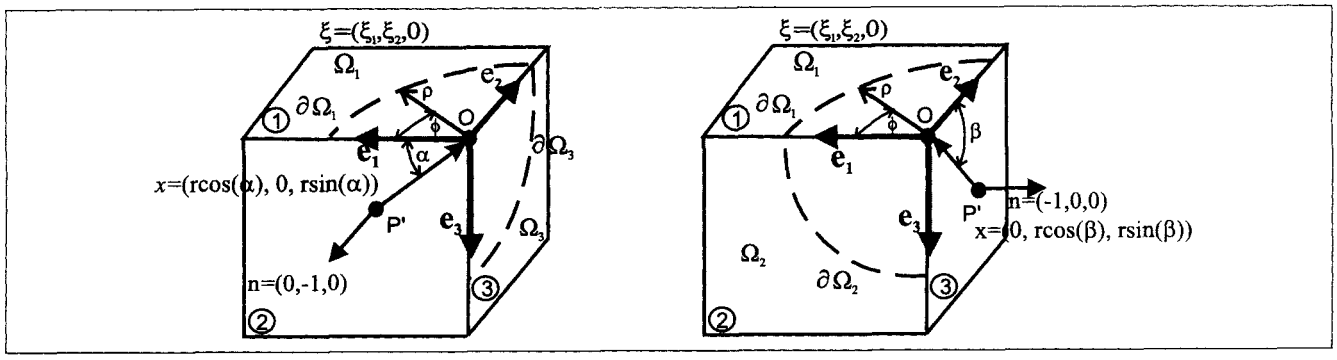

Figure 4. Vertex: definition of the local coordinate systems, for the traction problem.

vertex. For problems *with slip* boundary conditions, additional terms must be retained in the constitutive equation and $\boldsymbol{h}$ will depend parametrically on γ. This complication does not occur in our present problem and the problem of finding $q = -(\gamma - 1)$ is considerably easier.

It is clear from Eq. 24 that the traction field can be singular for values of $Re(\gamma) < 1$. Moreover, limits on γ follow from the requirement that the energy (strain energy for elasticity, rate of viscous dissipation for Stokes flow) should remain finite in the vertex region and this yields $Re(\gamma - 1) > -3/2$. However, for velocities to remain finite we require $Re(\gamma - 1) > -1$. In 3-D problems traction exponents less than -1 are admissible, leading to infinite velocities; in the present as well as other similar works (Bažant and Estenssoro, 1979; Benthem, 1980; Ghahremani, 1991) no roots less than -1 were found. (In 2-D flows, both the finite velocity and energy conditions lead to the identical constraint $Re(\gamma - 1) > -1$.)

We now proceed to apply the continuation method of Rosen and Cormack (1995). Consider the simplest case, namely, the vertex of a cube formed by three planes intersecting each other at 90° and the edges aligned with a rectangular Cartesian coordinate system, as shown in Figure 4. Even with the simplest case, the analysis is more difficult than that for the 2-D edge. For example, as the line segment $P'O$ is not orthogonal to the plane of integration (the $\xi_1\xi_2$ plane of Figure 4), we have been unable to obtain closed-form analytic expressions for the gauge integrals.

Since we have three planes with an unknown vector on them, there are 6×6 different gauge integrals. However, due to symmetry, only 12 are independent with the rest given by simple permutation of coordinate labels. On Figure 4, we show the two cases for the placement of the collocation points (Case I, the collocation point is on the xz plane; Case II, the collocation point is on the yz plane). Each case gives rise to six gauge integrals with the integration over the circle quadrant (Figure 4).

In case I we have

$$\boldsymbol{\xi} = (\xi_1, \xi_2, 0) \quad \boldsymbol{x} = (r\cos\alpha, 0, r\sin\alpha) \quad \boldsymbol{n} = (0, -1, 0) \tag{25}$$

Using polar coordinates based on the vertex, we define the auxiliary operators

$$I_{11}^{xz} = \int_0^\infty r^{q-1} \int_0^{\pi/2} \frac{\sin(\phi)\cos(\phi)^2(\cdot)}{R^{5/2}} d\phi dr \tag{26}$$

$$I_{12}^{xz} = \int_0^\infty r^{q-1} \int_0^{\pi/2} \frac{\cos(\phi)\sin(\phi)^2(\cdot)}{R^{5/2}} d\phi dz \tag{27}$$

$$I_{13}^{xz} = \int_0^\infty r^{q} \int_0^{\pi/2} \frac{\cos(\phi)\sin(\phi)(\cdot)}{R^{5/2}} d\phi dr \tag{28}$$

$$I_{22}^{xz} = \int_0^\infty r^{q-1} \int_0^{\pi/2} \frac{\sin(\phi)^3(\cdot)}{R^{5/2}} d\phi dr \tag{29}$$

$$I_{23}^{xz} = \int_0^\infty r^{q} \int_0^{\pi/2} \frac{\sin(\phi)^2(\cdot)}{R^{5/2}} d\phi dr \tag{30}$$

$$I_{33}^{xz} = \int_0^\infty r^{q} \int_0^{\pi/2} \frac{\sin(\phi)(\cdot)}{R^{5/2}} d\phi dr \tag{31}$$

where R is given by

$$R = 1 + r^2 - 2\cos\phi\cos\alpha r.$$

The gauge functionals are now given by

$$GfI_{11}^{xz}(\alpha) = I_{22}^{xz} - 2\cos\alpha I_{23}^{xz} + I_{33}^{xz}\cos^2\alpha \tag{32}$$

$$GfI_{12}^{xz}(\alpha) = I_{12}^{xz} - I_{13}^{xz}\cos\alpha \tag{33}$$

$$GfI_{13}^{xz}(\alpha) = -I_{23}^{xz} + I_{33}^{xz}\cos\alpha\sin\alpha \tag{34}$$

$$GfI_{22}^{xz}(\alpha) = I_{11}^{xz} \tag{35}$$

$$GfI_{23}^{xz}(\alpha) = -I_{13}^{xz}\sin\alpha \tag{36}$$

$$GfI_{33}^{xz}(\alpha) = I_{33}^{xz}\sin\alpha \tag{37}$$

In case II we have

$$\xi = (\xi_1, \xi_2, 0) \quad \boldsymbol{x} = (0, r\cos\alpha, r\sin\alpha) \quad \boldsymbol{n} = (-1, 0, 0). \tag{38}$$

This is equivalent to flipping the x and y axis and the gauge functionals are given as

$$GfI_{11}^{yz}(\alpha) = I_{11}^{yz} \tag{39}$$

$$GfI_{12}^{yz}(\alpha) = I_{12}^{yz} - I_{13}^{yz}\cos\alpha \tag{40}$$

$$GfI_{13}^{yz}(\alpha) = -I_{13}^{yz}\sin\alpha \tag{41}$$

$$GfI_{22}^{yz}(\alpha) = I_{22}^{yz} - 2\cos\alpha I_{23}^{yz} + I_{33}^{yz}\cos^2\alpha \tag{42}$$

$$GfI_{23}^{yz}(\alpha) = -I_{23}^{yz} + I_{33}^{yz}\cos\alpha\sin\alpha \tag{43}$$

$$GfI_{33}^{yz}(\alpha) = I_{33}^{yz}\sin\alpha \tag{44}$$

The operators I_{ij}^{yz} are now defined as

$$I_{11}^{yz} = \int_0^\infty r^{q-1} \int_0^{\pi/2} \frac{\cos(\phi)\sin(\phi)^2(\cdot)}{R^{5/2}} d\phi dr \tag{45}$$

$$I_{12}^{yz} = \int_0^\infty r^{q-1} \int_0^{\pi/2} \frac{\sin(\phi)\cos(\phi)^2(\cdot)}{R^{5/2}} d\phi dz \tag{46}$$

$$I_{13}^{yz} = \int_0^\infty r^{q} \int_0^{\pi/2} \frac{\sin(\phi)\cos(\phi)(\cdot)}{R^{5/2}} d\phi dr \tag{47}$$

$$I_{22}^{yz} = \int_0^\infty r^{q-1} \int_0^{\pi/2} \frac{\cos(\phi)^3(\cdot)}{R^{5/2}} d\phi dr \tag{48}$$

$$I_{23}^{yz} = \int_0^\infty r^{q} \int_0^{\pi/2} \frac{\cos(\phi)^2(\cdot)}{R^{5/2}} d\phi dr \tag{49}$$

$$I_{33}^{yz} = \int_0^\infty r^{q} \int_0^{\pi/2} \frac{\cos(\phi)(\cdot)}{R^{5/2}} d\phi dr \tag{50}$$

where R is given by

$$R = 1 + r^2 - 2\sin\phi\sin\alpha r.$$

As the point P' moves to the vertex, the dominant terms in the Riesz-Rennerb equation balance if and only if

$$\begin{pmatrix} -2\pi/3 & 0 & 0 & GfI_{33}^{yz} & GfI_{23}^{yz} & GfI_{13}^{yz} & GfI_{22}^{xz} & GfI_{23}^{xz} & GfI_{12}^{xz} \\ 0 & -2\pi/3 & 0 & GfI_{23}^{yz} & GfI_{22}^{yz} & GfI_{12}^{yz} & GfI_{23}^{xz} & GfI_{33}^{xz} & GfI_{13}^{xz} \\ 0 & 0 & -2\pi/3 & GfI_{13}^{yz} & GfI_{12}^{yz} & GfI_{11}^{yz} & GfI_{12}^{xz} & GfI_{13}^{xz} & GfI_{11}^{xz} \\ GfI_{11}^{xz} & GfI_{12}^{xz} & GfI_{13}^{xz} & -2\pi/3 & 0 & 0 & GfI_{11}^{yz} & GfI_{13}^{yz} & GfI_{12}^{yz} \\ GfI_{12}^{xz} & GfI_{22}^{xz} & GfI_{23}^{xz} & 0 & -2\pi/3 & 0 & GfI_{13}^{yz} & GfI_{33}^{yz} & GfI_{23}^{yz} \\ GfI_{13}^{xz} & GfI_{23}^{xz} & GfI_{33}^{xz} & 0 & 0 & -2\pi/3 & GfI_{12}^{yz} & GfI_{23}^{yz} & GfI_{22}^{yz} \\ GfI_{22}^{yz} & GfI_{12}^{yz} & GfI_{23}^{yz} & GfI_{33}^{xz} & GfI_{13}^{xz} & GfI_{23}^{xz} & -2\pi/3 & 0 & 0 \\ GfI_{12}^{yz} & GfI_{11}^{yz} & GfI_{13}^{yz} & GfI_{13}^{xz} & GfI_{11}^{xz} & GfI_{12}^{xz} & 0 & -2\pi/3 & 0 \\ GfI_{23}^{yz} & GfI_{13}^{yz} & GfI_{33}^{yz} & GfI_{23}^{xz} & GfI_{12}^{xz} & GfI_{22}^{xz} & 0 & 0 & -2\pi/3 \end{pmatrix} \begin{pmatrix} h_1 \\ h_2 \\ h_3 \\ h'_1 \\ h'_2 \\ h'_3 \\ h''_1 \\ h''_2 \\ h''_3 \end{pmatrix} = 0 \quad (51)$$

Here $(-2\pi/3)h_i$ and $GfI_{ij}^{xz}h_k$ are evaluated at α and $GIf_{ij}^{yz}h_k$ are evaluated at $\beta = \pi/2 - \alpha$.

The function $\boldsymbol{h}$ should satisfy the singular conditions at the two edges, that is $\cos^{-p}(\alpha)$ for $\alpha \to \pi/2$ and $\sin^{-p}(\alpha)$ for $\alpha \to 0$. So, it is natural to factor out the higher order 2-D singularities. The rest of $\boldsymbol{h}$ is now regular so we may apply a spectral element discretization with respect to ϕ, that is, we let $h_i = \cos^{-p}\phi \sin^{-p}\phi H_i(\phi)$, where p is as shown in the previous section and $H_i = \sum_{e=1}^{E}\sum_{j=1}^{N} a_j^e N_j^e(u)$, where $N_j^e(u)$ is a Lagrangian interpolant on N Gauss-Legendre-Lobatto points. The discretization of Eq. 51 will create a $(9 \times N_t) \times (9 \times N_t)$ system of linear equations, where N_t is the total number of collocation points.

Now we turn our attention to finding the values of q that satisfy the discretized version of Eq. 51. We have employed two different methods to help insure the veracity of our results. In the first, we use an eigenvalue solver that is particularly efficient in solving for the smallest eigenvalue (ARPACK, Lehoucq et al., 1994) and try to find the value of q for which the minimum eigenvalue of the matrix A in Eq. 51 is zero. In essence, we apply a root finding algorithm for q, with the eigenvalue solver as part of the functional evaluation.

In the second method, matrix A is linearized around q_o

$$A(q) = A(q_o) + (q - q_o)A'(q_o), \quad (52)$$

and we solve a generalized eigenvalue problem for $\lambda_q = q - q_o$. We have to find the value of q for which the minimum eigenvalue $|\lambda_q|$ is zero. Both methods gave similar results, but the first method involved a smaller number of matrix manipulations.

The search for q_o can be restricted to the interval [0, 3/2] and, as expected, there are only two distinct roots {0.31877..., 0.62463...} as summarized in Table 1. The larger of the two roots is a double root, also as expected. The explanation lies within the symmetry of the cube with respect to the orientation of the uniform stream. For the vertex of the cube in the positive octant, the "splitting" flow in which the uniform stream is parallel to the (1, 1, 1) direction is responsible for the smaller root. Any uniform stream in the plane orthogonal to the (1, 1, 1) direction gives the larger root from the following symmetry argument. The uniform streams along the (−1, 0, 1), (0, 1, −1), and (1, −1, 0) all give the same q. However, any two of these vectors form a basis for that plane, so all vectors in that plane give rise to the same value of q. The symmetry implications for the vertex are thus different from that for the 2-D edge where we found three distinct roots associated with the three orthogonal directions for the uniform stream.

The symmetry considerations also provide a check on our numerical method for construction of $\boldsymbol{h}(\phi)$. The eigenvalue solver furnishes two linearly independent eigenvectors at the double root, for example, associated with the (1, −2, 1) and (−1, 0, 1) orientations of the uniform stream. From the second one, we use symmetry to construct the solutions for the (1, −1, 0) and (0, 1, −1) directions. The difference between these solutions should equal the eigenvector for the (1, −2, 1) solution, and this is indeed the case.

In Figure 5 we show the three h_i and three H_i functions for the top plane (plane 1). The results for the side planes 2 and 3 follow from the permutation of the labels

$$t_x^{(1)} = t_y^{(2)} = t_z^{(3)}$$
$$t_y^{(1)} = t_z^{(2)} = t_x^{(3)}$$
$$t_z^{(1)} = t_x^{(2)} = t_y^{(3)}, \quad (53)$$

as the h_i functions inherit the symmetry properties of the traction components.

Note that for the splitting flow at the vertex, the strongest singularity seen by the edges that meet at the vertex is $p = 1/3$ so that the appropriate decomposition of the tractions is

$$t_i = r^{-0.31877}h_i(\phi) = r^{-0.31877}\cos^{-1/3}\phi \sin^{-1/3}\phi H_i(\phi).$$

Now we turn our attention to the other flow. Here, we should mention that while the splitting flow exponent can be calculated very accurately with relatively few collocation points (such as 9 Gauss-Legendre points) the determination of the double eigenvalue is more difficult. The edges that meet at the vertex now have the exponent −0.455516 so that the numerical integrations are more difficult. On Figure 9 we show the linear convergence of the eigenvalue, for fifth order Gauss-Legendre elements. We obtain the reported results for q by extrapolation of the solution to an infinite number of nodes, as shown in Figure 9. We then have the result

$$t_i = r^{-0.6246}h_i(\phi) = r^{-0.6246}\cos^{-0.455516}\phi \sin^{-0.455516}\phi H_i(\phi).$$

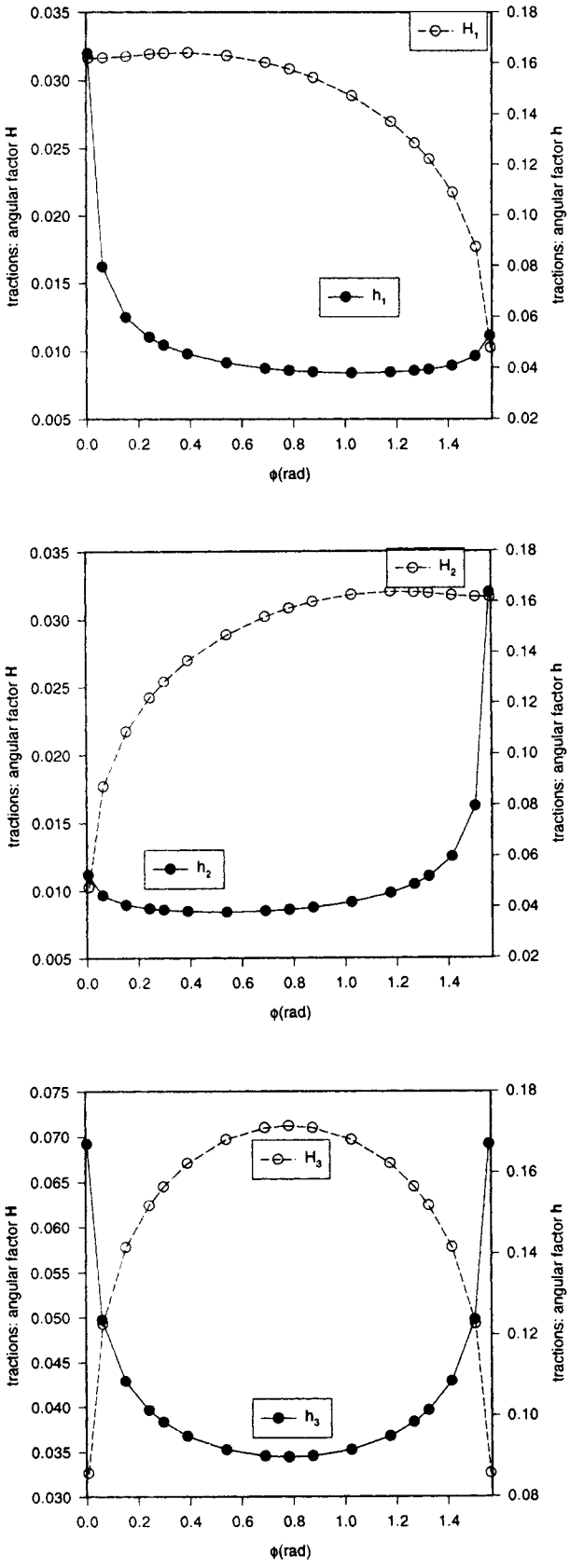

Figure 5. Eigenvectors at a cube vertex: (1, 1, 1), direction of the uniform stream, traction exponent $q = 0.31877$.

Circles denote the collocation points.

On Figures 6, 7, and 8 we show plots of the eigenvector (h_i and H_i functions) for this double root problem.

It is clear from this analysis that the traction field around a vertex possesses a stronger singularity than its 2-D counterpart. For a more general vertex formed by the intersection of three planes, the resolution of the stress field will require the determination of nine 2-D exponents and three 3-D components. This creates quite a challenge for computational strategies based on singular elements or subtraction of singularities.

Boundary Element Discretization

Now that we know the structure of the solution near the edges and vertices, we may formulate discretization strategies for the numerical solution of more general flow problems of microhydrodynamics. The numerical method for the traction field over the particle must be capable of tackling the singular behavior that is present near the edges and the vertices of the particle. Three major numerical boundary element discretization techniques have been used by our group, namely, lower order elements with adaptive discretization, spectral and B-Spline elements. The numerics could also be augmented with analytical or semi-analytical manipulation of these singularities. In general there are two techniques based in the (a) local analytical subtraction of the singularity, and (b) incorporation of the singular behavior into the trial function. The complexity of the geometry and the large number of singularities, both point and line, make the first technique inadmissible. Trial function modification has been applied successfully in 2-D problems like the stick-slip (Georgiou et al., 1991) and sudden expansion problem (Georgiou et al., 1990). On these problems, however, only one singular point is present. In the 3-D case of flow around a cubic particle, however, the presence of line singularities does not allow the concentration of singular triangular elements near the singularity. The presence of the vertex introduces an additional singularity potentially stronger than the line type. As we have seen the traction field near the vertex should be

$$t_i(\theta) = r^{-q}\rho^{-p_j}\rho'^{-p'_k} f(\theta) \tag{54}$$

where r is the distance from the vertex, and ρ, ρ' are the distances from the line singularities on the same plane with respective exponents p_j, p'_j given by the 2-D analysis. Since q is different and in general greater than p_j or p'_j, it becomes apparent that the simple tensor products of singular basis elements will fail to resolve the traction field. Moreover, most of the elements in the discretization should have the singular basis. However, the introduction of the singular terms in the trial function destroys the orthogonality and gives rise to numerical difficulties. In addition, as we have seen, the determination of the exponent of the 3-D singularity q requires the solution of a nonlinear eigenvalue problem. One additional disadvantage of this treatment is that the trial functions will be bounded on the specific geometry. Thus, in order to apply the method on a more general polyhedron (like a truncated pyramid) we need to deploy different basis functions on each particle face, thereby increasing dramatically the complexity of the problem. Other techniques like the mapping of the singular point into a nonsingular domain

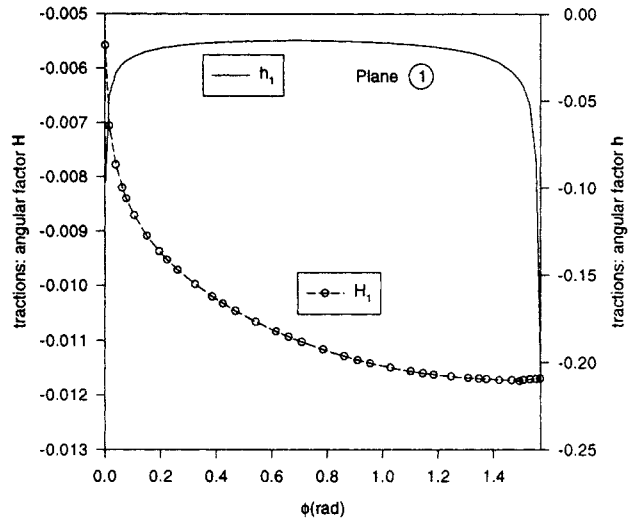

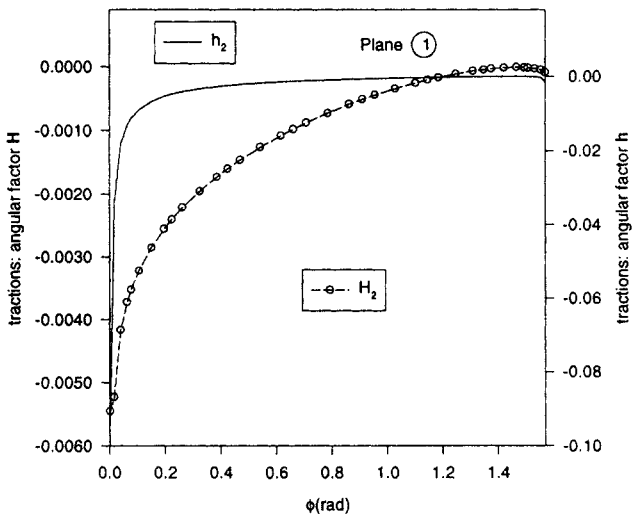

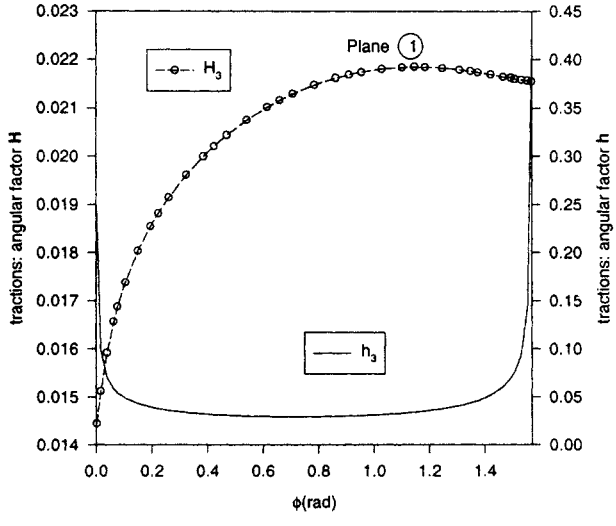

Figure 6. x-component of the eigenvector at the cube vertex, direction of the uniform stream: (−1, 0, 1), traction exponent $q = 0.62463$.

Circles denote the collocation points.

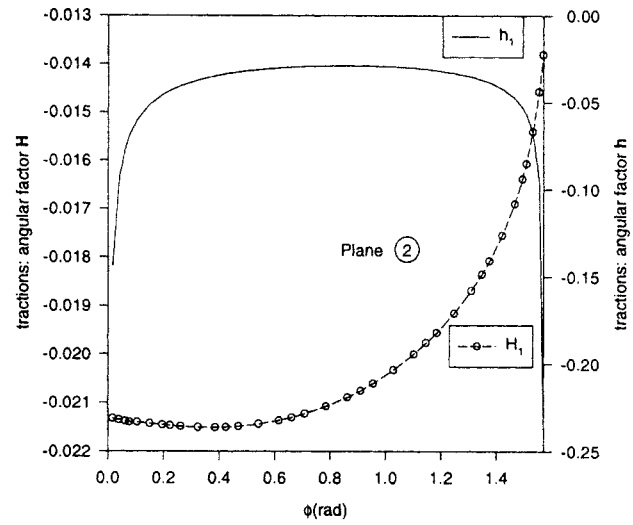

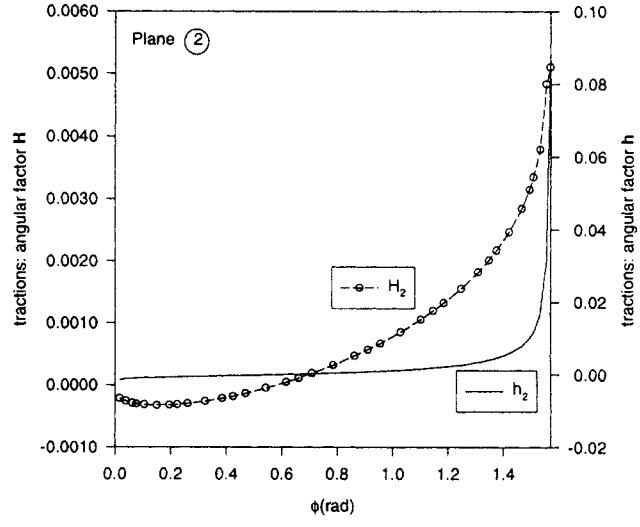

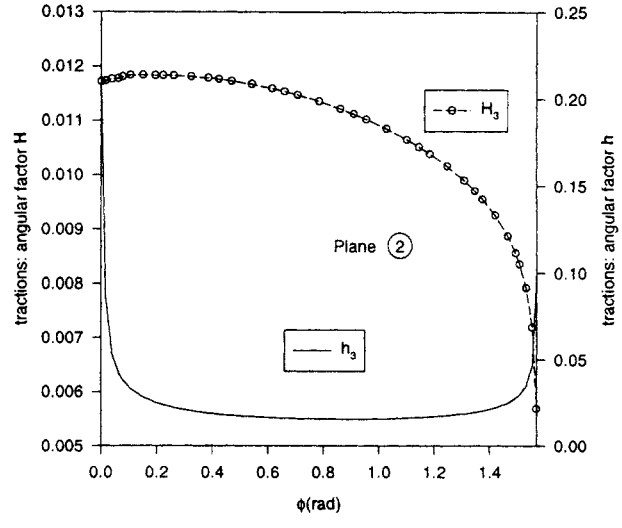

Figure 7. y-component of the eigenvector at the cube vertex, direction of the uniform stream: (−1, 0, 1), traction exponent $q = 0.62463$.

Circles denote the collocation points.

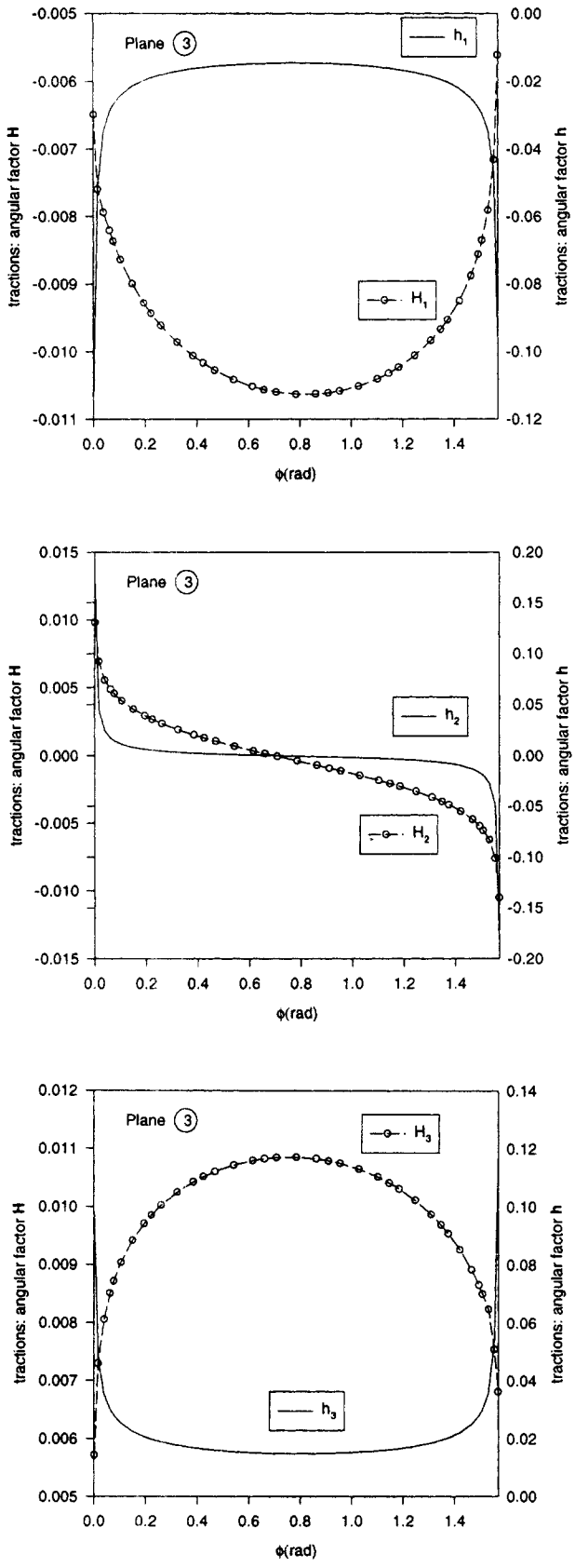

Figure 8. z-component of the eigenvector at the cube vertex, direction of the uniform stream: (−1, 0, 1), traction exponent $q = 0.62463$.

Circles denote the collocation points.

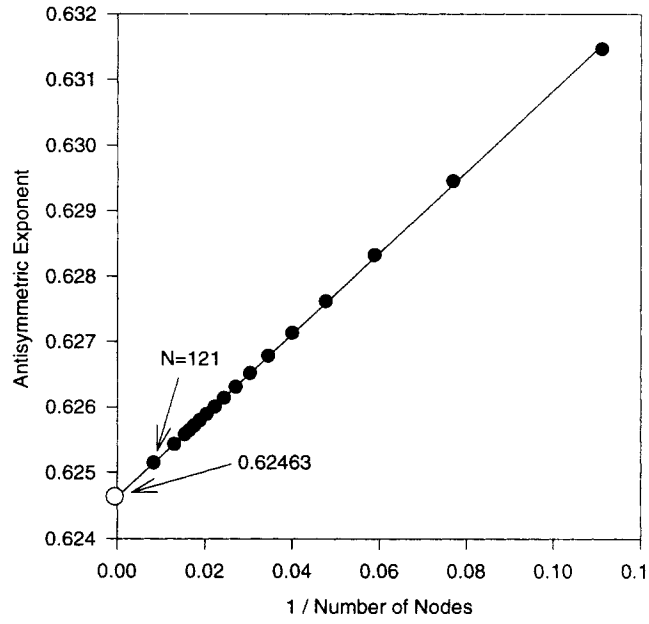

Figure 9. Vertex: Extrapolation for the calculation of the exponent from the double root.

(Pathria and Karniadakis, 1995) cannot be applied effectively due to the number of singular mappings needed.

An alternative is the use of regular interpolation methods with the application of a gap between the last collocation point and the vertex or edge of the particle. The gap is necessary in order to produce both the discontinuity of the double layer density and approximate the correct singular behavior of the traction field. The application of the gap does not need to be physical as in Pakdel and Kim (1996), meaning that both the integration and the geometry representation can cover the edges and only the last collocation point is moved inside. Ideal candidates for this polynomial interpolation scheme are the Chebyshev or Legendre orthogonal polynomials since they avoid the boundaries of the elements. Of course, since the approximation of a singular field is left to a regular polynomial basis the exponential convergence is lost and a large number of collocation points is needed.

Numerical Simulation for the Traction Field

In this section we present the numerical results based on the boundary element analysis. The details of the discretization strategies are available in Mustakis (1998). Specific flows that isolate the fundamental flows around the edges and vertices of a cube are studied.

Edges

We have seen already that the integral equation is fully capable of producing the singular behavior of the traction field. The question is whether the numerical solution does that correctly as well. First, we consider the 2-D case across the edges of the cube. In Figure 10 we define two simple flows: (a) normal to the face of a cube; and (b) splitting to the cube edge. These flows are easiest to analyze since they possess only one active exponent on specific edges. For example, flow (a) exhibits parallel flow along the edge and so the trac-

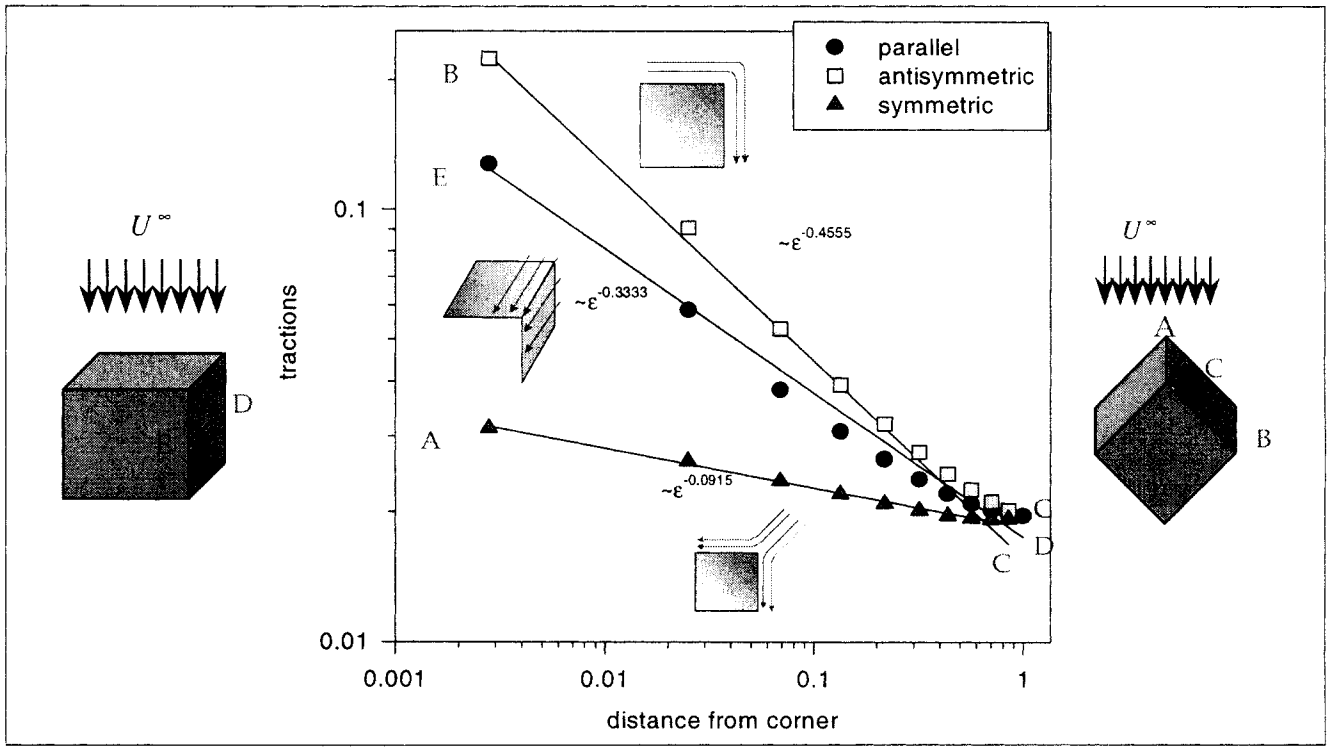

Figure 10. Traction singularities for an edge of $\pi/2$ angle.

Discretization is 12 8×8 Chebyshev Spectral Elements.

tion field should have a -0.33333 singularity exponent. For the splitting flow, the splitting edge (A) has only the symmetric component and the traction along AC should follow the -0.0915 singularity, whereas the edge across the face (B) has only the antisymmetric component and the tractions along CB exhibit the -0.4555 exponent. Here, we should mention that we concentrate our attention on the middle of the edges in order to minimize the effects from the vertex region.

Discretizations with spectral elements are able to reconstruct the singular traction fields for these test flows (Figure 10). This came as a pleasant surprise since one expects the spectral solutions (and for that matter any polynomial discretization) to oscillate as it approaches the singular point. On the contrary, the recovery of the singularity exponents is almost perfect. The traction field, as we move closer to the edges, is almost smooth. Small oscillations are present close to the singularity, but if we consider values at just the collocation points the solution is smooth as shown in Figure 10. This demonstrates the power of the spectral elements and the near optimal recovery property of the Chebyshev collocation points. Similar results were obtained from the B-Spline elements. In contrast, and as expected, the lower-order methods, such as quadratic and linear elements, fared poorly and only very high discretizations produced meaningful results (more than 5,000 nodes).

Vertices

Now we turn our attention to the numerical solution of flows near the vertex. We have examined three different flow conditions corresponding to the three eigenvalues (-0.318, -0.624 double). These flows are the $\boldsymbol{u}=(-1,-1,-1)$, $\boldsymbol{u}=(-1,0,1)$ and $\boldsymbol{u}=(-1,2,-1)$ corresponding to the symmetric, antisymmetric mode I and antisymmetric mode II, respectively for the vertex located (1, 1, 1). We present in Figures 11, 12, and 13 the tractions along the diagonal of the top plane.

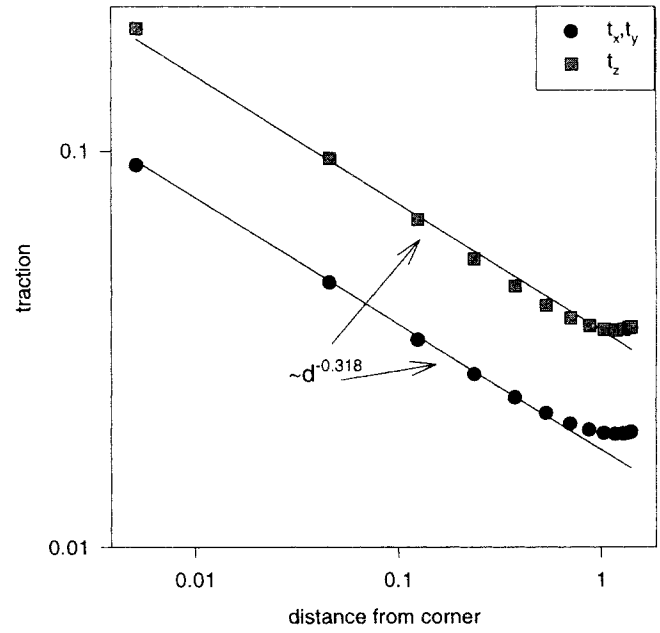

Figure 11. Symmetric flow $\boldsymbol{u}=(-1,-1,-1)$ on vertex (1, 1, 1).

Tractions along the diagonal of the top plane.

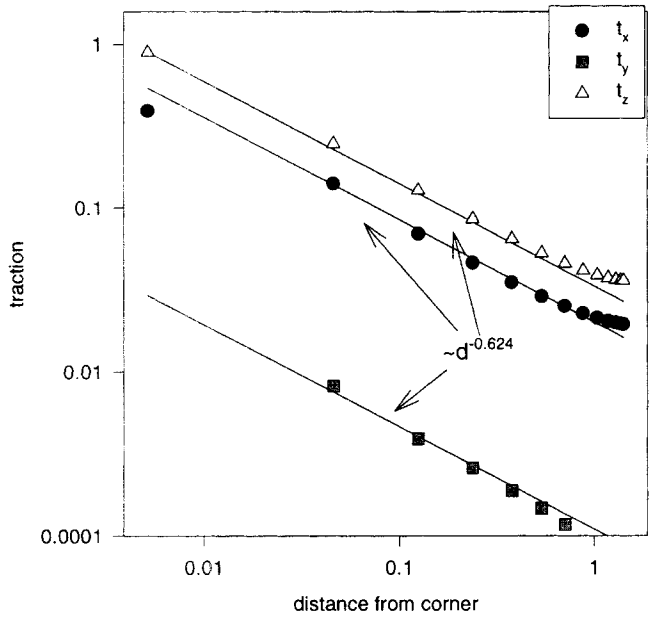

Figure 12. Antisymmetric flow, mode I $u = (-1, 0, 1)$ on vertex (1, 1, 1).

Tractions along the diagonal of the top plane.

In Figure 11 we see that the BIEM discretization with spectral elements is able to capture the singular behavior of the traction field, that is, the traction exponent -0.318 is reproduced with a $\pm 5\%$ accuracy. The same is true for the mode II antisymmetric flow with the -0.624 exponent (Figure 13). However, for the mode I antisymmetric flow (Figure 12) and the t_y exponent, the method overpredicts the exponent with an error of more than 30%, whereas the two other

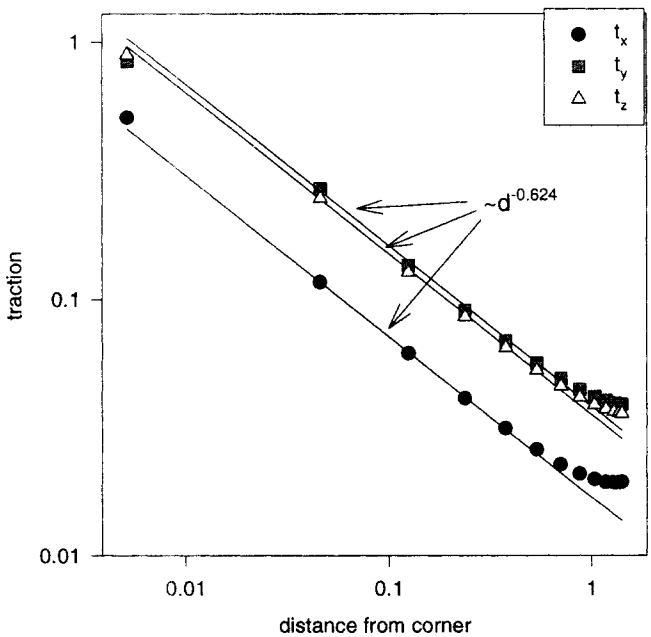

Figure 13. Antisymmetric flow, mode II $u = (-1, 2, -1)$ on vertex (1, 1, 1).

Tractions along the diagonal of the top plane.

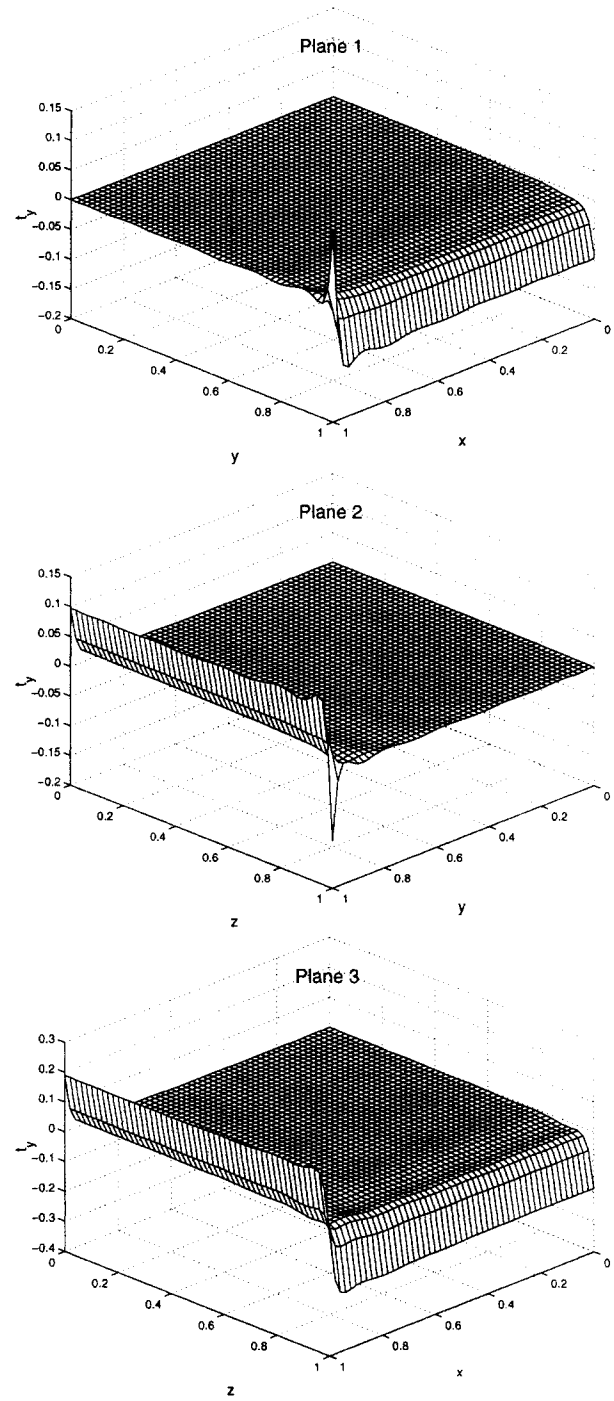

Figure 14. t_y on the (1, 1, 1) vertex, the tree planes, flow vector $u = (-1, 0, 1)$, Gauss-Chebyshev 10th order.

components (t_x, t_z) are in good agreement. The reason becomes apparent if we examine the traction field across the third plane of the vertex (1, 1, 1). Figure 14 displays the t_y exponents on all three planes (the numbering scheme for the planes is given in Figure 4). As we can see on planes 1 and 2, t_y is almost zero except very close to the vertex where it possesses oscillations. On plane 3, however, t_y is smooth and, if we move along the diagonal, is equal to zero, as expected from the continuation analysis. However, on plane 3 any other

approach except the diagonal should result in a value approaching either $-\infty$ or $+\infty$, a situation which cannot be modeled with the current discretization. BIEM breaks down at that point, and oscillations appear in the solution. Fortunately, because the values of t_y are small, they do not contaminate the other two components t_x and t_y. It is apparent that for these flow conditions special attention should be paid to the vertex. Two possibilities are open: (a) use special discretization on the vertex with elements that utilize the three eigenvectors. This method leads to problem-specific discretization; (b) remove the continuity requirements on the vertex node. The easiest way to do that is deployment of triangular elements on the vertex with relaxation of the inter-element continuity.

Conclusions

The traction field for particles with sharp corners and edges (such as a cube) exhibits singular behavior in contrast to the smooth field on simpler particle geometries (spheres). The boundary integral equation of the second kind can handle such singular behavior. Asymptotic analysis of the integral equation near the edges of the particle reproduces the streamfunction results. The vertices present a more formidable challenge; the traction field exhibits an even higher singularity on top of those emanating from the edges that create the vertex. The asymptotic analysis on the vertex region extracts these new singular exponents and identifies a canonical set of ambient basis flows around a vertex. Numerical discretizations using low-order, spectral, and B-Spline elements produce results that are in good agreement with those obtained from the asymptotic analysis. This demonstrates the accuracy and robustness of the numerical methods based on the second kind integral representation for Stokes flow. In general, the full traction field of the translating or rotating particle can be integrated to recover the particles' mobility in agreement with results in the literature (Pettyjohn and Christiansen, 1948). In future articles, we will employ these methods to provide a complete description of the hydrodynamic interaction between sharp objects in a viscous fluid.

Acknowledgments

This material is based on work supported by LG Oil and Grant CTS-9520403 from the NSF GOALI Program. We also like to thank Prof. D. E. Cormack (University of Toronto) and Prof. W. J. Drugan (University of Wisconsin-Madison) for helpful comments on the continuation method and related works in the elasticity literature.

Literature Cited

Abramowitz, M., and I. A. Stegun, *Handbook of Mathematical Functions*, Dover Publications, New York (1970).

Bažant, Z. P., and L. F. Estenssoro, "Surface Singularity and Crack Propagation," *Int. J. Solids Structures*, **15**, 403 (1979).

Benthem, J. P., "State of Stress at the Vertex of a Quarter-Infinite Crack in a Half-Space," *Int. J. Solids Structures*, **13**, 479 (1977).

Benthem, J. P., "The Quarter-Infinite Crack in a Half-Space; Alternative and Additional Solutions," *Int. J. Solids Structures*, **16**, 119 (1980).

Bird, R. B., W. E. Stewart, and E. N. Lightfoot, *Transport Phenomena*, Wiley, New York (1960).

Brenner, H., "The Stokes Resistance of an Arbitrary Particle: IV. Arbitrary Fields of Flow," *Chem. Eng. Sci.*, **19**, 703 (1964).

Cormack, D. E., and D. Rosen, "Gauge Conditions and the Analysis of Singular Fields with Boundary Integral Equations," *Eng. Anal. Boundary Elements*, **18**, 1 (1996).

Dean, W. R., and P. E. Montagnon, "On the Steady Motion of Viscous Liquid in a Corner," *Proc. Camb. Phil. Soc.*, **45**, 389 (1949).

Georgiou, G. C., W. W. Schultz, and L. G. Olson, "Singular Finite Elements for the Sudden-Expansion and the Die-Swell Problems," *Int. J. Numer. Meth. Fluids*, **10**, 357 (1990).

Georgiou, G. C., L. G. Olson, and W. W. Schultz, "The Integrated Singular Basis Function Method for the Stick-Slip and the Die-Swell Problems," *Int. J. Numer. Meth. Fluids*, **13**, 1251 (1991).

Ghahremani, F., "A Numerical Variational Method for Extracting 3D Singularities," *Int. J. Solids Structures*, **27**(11), 1371 (1991).

Happel, J., and H. Brenner, *Low Reynolds Number Hydrodynamics*, Martinus Nijhoff, The Hague, The Netherlands (1983).

Karniadakis, G. E., "Spectral Element Simulations of Laminar and Turbulent Flows in Complex Geometries," *Appl. Numer. Meth.*, **6**, 85 (1989).

Karrila, S. J., "Linear Operator Theory Applied to Fast Computational Strategies for Particle Interactions in Viscous Flows," PhD thesis, University of Wisconsin-Madison (1988).

Kim, S., and S. J. Karrila, *Microhydrodynamics: Principles and Selected Applications*, Butterworth-Heinemann, Boston (1991).

Kim, S., and H. Power, "A Note on Two Boundary Integral Formulations for Particle Mobilities in Stokes Flow," *J. Fluid Mech.*, **257**, 637 (1993).

Kondratev, V. A., "Boundary Problems for Elliptic Equations with Conical or Angular Points," *Trans. Moscow Math. Soc.*, **17**, 209 (1968).

Ladyshenskaya, O. A., *The Mathematical Theory of Viscous Incompressible Flow*, Gordon and Breach, New York (1963).

Lehoucq, R., D. C. Sorensen, and P. A. Vu, "ARPACK: Fortran Subroutines for Solving Large Scale Eigenvalue Problems," Release 2.1, available from netlib@ornl.gov in the scalpack directory (1994).

Liu, Y., D. F. Evans, Q. Song, and D. W. Grainger, "Structure and Frictional Properties of Self-Assembled Surfactant Monolayers," *Langmuir*, **12**, 1235 (1996).

Moffatt, H. K., "Viscous and Resistive Eddies Near a Sharp Corner," *J. Fluid Mech.*, **18**, 1 (1964).

Mustakis, I., "Microhydrodynamics of Sharp Corners and Edges," PhD Thesis, University of Wisconsin-Madison (available on the World Wide Web at http://calypso.che.wisc.edu/~ iasonas/aichepaper.html) (1998).

Nakamura, T., and D. M. Parks, "Antisymmetrical 3-D Stress Field Near the Crack Front of a Thin Elastic Plate," *Int. J. Solids Structures*, **25** (12), 1411 (1989).

Odqvist, F. K. G., "Über die Randwertaufgaben der Hydrodynamik zäher Flüssigkeiten (On the Boundary Value Problems in Hydrodynamics of Viscous Fluids), *Math. Z.*, **32**, 329 (1930).

Pakdel, P., and S. Kim, "Traction Singularities on Sharp Corners and Edges in Stokes Flows," *Chem. Eng. Comm.*, 148–150, 257 (1996).

Pathria, D., and G. E. Karniadakis, "Spectral Element Methods for Elliptic Problems in Non-Smooth Domains," *J. Comput. Phys.*, **122**, 83 (1995).

Pettyjohn, E. S., and E. B. Christiansen, "Effect of Particle Shape on Free-Settling Rates of Isometric Particles," *Chem. Eng. Prog.*, **44**, 157 (1948).

Pozrikidis, C., *Boundary Integral and Singularity Methods for Linearized Viscous Flow*, Cambridge Univ. Press, London (1991).

Rosen, D., and D. E. Cormack, "On the Corner Analysis in the BEM by the Continuation Approach," *Eng. Anal. Boundary Elements*, **16**, 53 (1995).

Russel, W. B., W. R. Schowalter, and D. A. Saville, *Colloidal Dispersions*, Cambridge Univ. Press, London (1989).

Williams, M. L., "Stress Singularities Resulting from Various Boundary Conditions in Angular Corners of Plates in Extention," *J. Appl. Mech.*, **19**, 526 (1952).

Appendix: Integral Equation for Tractions

In this appendix, we summarize the direct method for computing the surface tractions, as described in Karrila and Kim

(1989), Chapter 17 of Kim and Karrila (1991), and Kim and Power (1993).

Traction Computations with Completed Double Layer

Brenner (1964) was the first to show that as a consequence of the Lorentz reciprocal theorem, the drag on a particle in arbitrary ambient Stokes flow $\boldsymbol{v}^{\infty}$ is related to the tractions for a particle in rigid body motion

$$e_i \cdot \boldsymbol{F} = \langle (\boldsymbol{\sigma}^{\mathrm{RBM}} \cdot \boldsymbol{n})^{(i)}, \boldsymbol{v}^{\infty} \rangle \tag{A1}$$

Here $(\boldsymbol{\sigma}^{\mathrm{RBM}} \cdot \boldsymbol{n})^{(i)}$ is the surface traction of the disturbance field produced when the particle is in rigid body translation in the ith coordinate direction. If we interpret the inner product as a linear functional mapping $\boldsymbol{v}^{\infty}$ to $\boldsymbol{F}$ then, according to the Riesz representation theorem, $(\boldsymbol{\sigma}^{\mathrm{RBM}} \cdot \boldsymbol{n})^{(i)}$ is the unique vector that performs this role.

This idea applies to mobility problems as well. Consider the linear functional that maps

$$\boldsymbol{b} = \left[\boldsymbol{F} - \frac{1}{2} (\boldsymbol{T} \times \nabla) \right] \cdot \frac{\mathcal{G}(\boldsymbol{x})}{8\pi\mu} \rightarrow \langle \boldsymbol{\varphi}, \boldsymbol{\varphi}^{(\ell)} \rangle, \qquad \ell = 1, 2, \ldots 6.$$

By the Riesz representation theorem, there is a unique $\boldsymbol{t}^{(\ell)}$ that satisfies

$$\langle \boldsymbol{\varphi}, \boldsymbol{\varphi}^{(\ell)} \rangle = \langle \boldsymbol{b}, \boldsymbol{t}^{(\ell)} \rangle$$

for all $\boldsymbol{b}$.

Here we rewrite Eq. 3 as

$$\varphi(\boldsymbol{x}) + \mathcal{K}(\varphi) = \boldsymbol{b} \tag{A2}$$

where $\mathcal{K}$ is an operator defined as

$$\mathcal{K}(\cdot) = \mathcal{K}(\cdot) + \oint_S \left(\sum_{\ell} \boldsymbol{\varphi}^{(\ell)} \boldsymbol{\varphi}^{(\ell)} \right) \cdot (\cdot) dS = \oint_S \left(\mathcal{K} + \sum_{\ell} \boldsymbol{\varphi}^{(\ell)} \boldsymbol{\varphi}^{(\ell)} \right) \cdot (\cdot) dS$$

If we restrict our attention to $\boldsymbol{b}$ in the range of $1 + \mathcal{K}$, then Eq. A2 implies

$$\langle \boldsymbol{\varphi}, \boldsymbol{\varphi}^{(\ell)} \rangle = \langle \boldsymbol{b}, \boldsymbol{t}^{(\ell)} \rangle = 0, \qquad \boldsymbol{b} \in R(1 + \mathcal{K}).$$

Thus, $\boldsymbol{t}^{(\ell)} \perp R(1 + \mathcal{K})$ and the Fredholm alternative leads to $\boldsymbol{t}^{(\ell)} \in N(1 + \mathcal{K}^*)$, that is, as expected, $\boldsymbol{t}^{(\ell)}$, $\ell = 1, 2, \ldots, 6$ are the six tractions associated with the disturbance velocity produced by the six independent rigid body motion of the particle. The equation for computing these tractions is readily derived by taking the inner product of $\boldsymbol{t}^{(\ell)}$ with Eq. 3, resulting in

$$\langle \boldsymbol{b}, \boldsymbol{t}^{(\ell)} \rangle = \sum_{i=1}^{6} \langle \boldsymbol{\varphi}^{(i)}, \boldsymbol{t}^{(\ell)} \rangle \langle \boldsymbol{\varphi}, \boldsymbol{\varphi}^{(\ell)} \rangle = \left\langle \boldsymbol{\varphi}, \sum_{i=1}^{6} \langle \boldsymbol{\varphi}^{(i)}, \boldsymbol{t}^{(\ell)} \rangle \boldsymbol{\varphi}^{(i)} \right\rangle$$

Replacing $\boldsymbol{b} = (1 + \mathcal{K})\boldsymbol{\varphi}$ in this relation then yields

$$\langle (1 + \mathcal{K})\boldsymbol{\varphi}, \boldsymbol{t}^{(\ell)} \rangle = \langle \boldsymbol{\varphi}, (1 + \mathcal{K}^*)\boldsymbol{t}^{(\ell)} \rangle = \left\langle \boldsymbol{\varphi}, \sum_{i=1}^{6} \langle \boldsymbol{\varphi}^{(i)}, \boldsymbol{t}^{(\ell)} \rangle \boldsymbol{\varphi}^{(i)} \right\rangle$$

so that the governing equation for $\boldsymbol{t}^{(\ell)}$ is

$$(1 + \mathcal{K}^*)\boldsymbol{t}^{(\ell)} = \sum_{i=1}^{6} \langle \boldsymbol{\varphi}^{(i)}, \boldsymbol{t}^{(\ell)} \rangle \boldsymbol{\varphi}^{(i)}. \tag{A3}$$

This result is Eq. 17.91 of Kim and Karrila (1991) except for minor changes in notation. We insert the explicit expressions for the $\boldsymbol{\varphi}^{(i)}$

$$\boldsymbol{\varphi}^{(1)} = \boldsymbol{e}_1/\sqrt{S}, \qquad \boldsymbol{\varphi}^{(2)} = \boldsymbol{e}_2/\sqrt{S}, \qquad \boldsymbol{\varphi}^{(3)} = \boldsymbol{e}_3/\sqrt{S}, \tag{A4}$$

$$\boldsymbol{\varphi}^{(4)} = (\boldsymbol{e}_1 \times \boldsymbol{r})/\sqrt{I_1}, \qquad \boldsymbol{\varphi}^{(5)} = (\boldsymbol{e}_2 \times \boldsymbol{r})/\sqrt{I_2}, \qquad \boldsymbol{\varphi}^{(6)} = (\boldsymbol{e}_3 \times \boldsymbol{r})/\sqrt{I_3}, \tag{A5}$$

so that

$$\sum_{i=1}^{3} \langle \boldsymbol{\varphi}^{(i)}, \boldsymbol{t}^{(\ell)} \rangle \boldsymbol{\varphi}^{(i)} = \frac{1}{S} \sum_{i=1}^{3} \oint_S \boldsymbol{e}_i \boldsymbol{e}_i \cdot \boldsymbol{t}^{(\ell)} dS = \frac{1}{S} \boldsymbol{F}$$

and

$$\sum_{i=4}^{6} \langle \boldsymbol{\varphi}^{(i)}, \boldsymbol{t}^{(\ell)} \rangle \boldsymbol{\varphi}^{(i)} = \left(\frac{T_2 r_3}{I_2} - \frac{T_3 r_2}{I_3} \right) \boldsymbol{e}_1 + \left(\frac{T_3 r_1}{I_3} - \frac{T_1 r_3}{I_1} \right) \boldsymbol{e}_2 + \left(\frac{T_1 r_2}{I_1} - \frac{T_2 r_1}{I_2} \right) \boldsymbol{e}_3.$$

Equation A3 can thus be expressed in the final form

$$t_i + \oint_S H_{ij}^* t_j dS = \frac{1}{S} F_i + \epsilon_{ijk} \left(\frac{T_j}{I_j} \right) r_k \tag{A6}$$

A straightforward extension to multiparticle systems gives Eq. 6. The solution of the traction field now can be obtained as the fixed point of a convergent iterative scheme.

Manuscript received Dec. 12, 1997, and revision received Apr. 20, 1998.